Inorganic Chemistry

pubs.acs.org/IC Article

Self-Assembled Encapsulation of CuX_2^- (X = Br, Cl) in a Gold Phosphine Box-like Cavity with Metallophilic Au−Cu Interactions

Daniel T. Walters, Michael M. Aristov, Reza Babadi Aghakhanpour, Daniel J. SantaLucia, Sarah Costa, Marilyn. M. Olmstead, John F. Berry,* and Alan. L. Balch*

Cite This: *Inorg. Chem.* 2023, 62, 4467−4475 Read Online

ACCESS | Metrics & More | Article Recommendations | Supporting Information

ABSTRACT: Synthetic routes to the crystallization of two new box-like complexes, $[Au_6(Triphos)_4(CuBr_2)](OTf)_5\cdot(CH_2Cl_2)_3\cdot(CH_3OH)_3\cdot(H_2O)_4$ (**1**) and $[Au_6(Triphos)_4(CuCl_2)](PF_6)_5\cdot(CH_2Cl_2)_4$ (**2**) (triphos = bis(2-diphenylphosphinoethyl)phenylphosphine), have been developed. The two centrosymmetric cationic complexes have been structurally characterized through single-crystal X-ray diffraction and shown to contain a CuX_2^- (X = Br or Cl) unit suspended between two Au(I) centers without the involvement of bridging ligands. These colorless crystals display green luminescence (λ_{em} = 527 nm) for (**1**) and teal luminescence (λ_{em} = 464 nm) for (**2**). Computational results document the metallophilic interactions that are involved in positioning the Cu(I) center between the two Au(I) ions and in the luminescence.

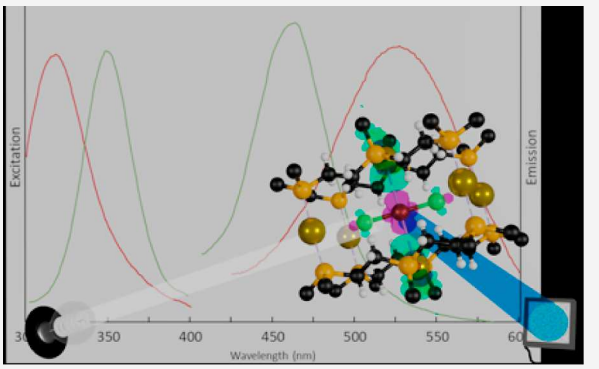

INTRODUCTION

Recent years have seen the synthesis of many cage-like molecules that can provide a closed interior space in which an array of atoms, ions, or other molecules can be encapsulated.[1−8] Such container molecules have been shown to be capable of trapping and protecting reactive molecules ranging from cyclobutadiene[9] to tetrahedral P_4.[10] The carbon cages of fullerenes have been found to encapsulate a range of atomic clusters such as Sc_4O_3,[11] Gd_2C_2,[12] and U_2N[13] that have no terrestrial existence outside of the fullerene cage. Luminescent cage molecules can be made by the incorporation of fluorescent or phosphorescent components into the fabric of the cage.[14] The emissive properties of such cages may be perturbed by encapsulation of other molecules or ions. Thus, these cages may be utilized as sensors. Porous cage molecules that allow smaller molecules to pass through the interior are well equipped to function as catalysts.[1] For example, a cage-confined photocatalyst has been developed for the [2 + 2] cycloaddition of α,β-unsaturated carbonyl compounds.[15]

A short while ago, we discovered that luminescent, self-assembled box-like molecules could be constructed from non-luminescent components: the tridentate ligand bis(2-diphenylphosphinoethyl)phenylphosphine (Triphos), gold(I) ions, and chloride or bromide ions.[16,17] Scheme 1 summarizes prior work on these luminescent boxes. The chloro-box involves the cation, $[Au_6(Triphos)_4Cl]^{5+}$, which displays a readily observed blue emission at room temperature. While three-coordinate gold(I) complexes are usually highly emissive,[18−20] the distances between the gold(I) ion and the two neighboring chloride ions are rather long, ca 3.50 Å, in these chloro-box cations. Consequently, the emission of this box has been suggested to involve the production of an exciplex formed by the interaction of the gold ions with the adjacent chloride ion at the center of the box. Additionally, these salts, $[Au_6(Triphos)_4Cl](EF_6)_5\cdot n(CH_3C_6H_5)$ (E = P, As, or Sb), are mechanochromic[21−25] and are transformed into the chloro-bridged helicate dimer upon grinding. A relatively simple mechanism involving the breaking of only two Au−P bonds has been proposed to account for this mechanochromic transformation.

Similar box-like molecules have been made by the addition of bromide ions to the helicate tri-gold complex, $[Au_3(Triphos)_2](O_3SCF_3)_3$,[26] and contain either one or two bromide ions.[12] Both the mono-bromo-box and the di-bromo-box salts are luminescent. Crystals of the mono-bromo-box, $[Au_6(Triphos)_4Br](SbF_6)_5\cdot 6(CH_2Cl_2)$, are mechanochromic and are transformed by grinding into a solid containing the non-luminescent bromo-bridged helicate dimer, $[(\mu\text{-Br})\text{-}\{Au_3(Triphos)_2\}_2]^{5+}$.

Here we explore another aspect of the chemistry of these box-like cations. Remarkably, we have discovered that the anions $CuCl_2^-$ and $CuBr_2^-$ can be trapped within these gold

Received: November 17, 2022
Published: March 10, 2023

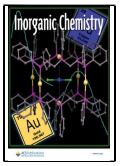

https://doi.org/10.1021/acs.inorgchem.2c04067
Inorg. Chem. 2023, 62, 4467−4475

Scheme 1. Formation of Gold Box and Helicate Cations[a]

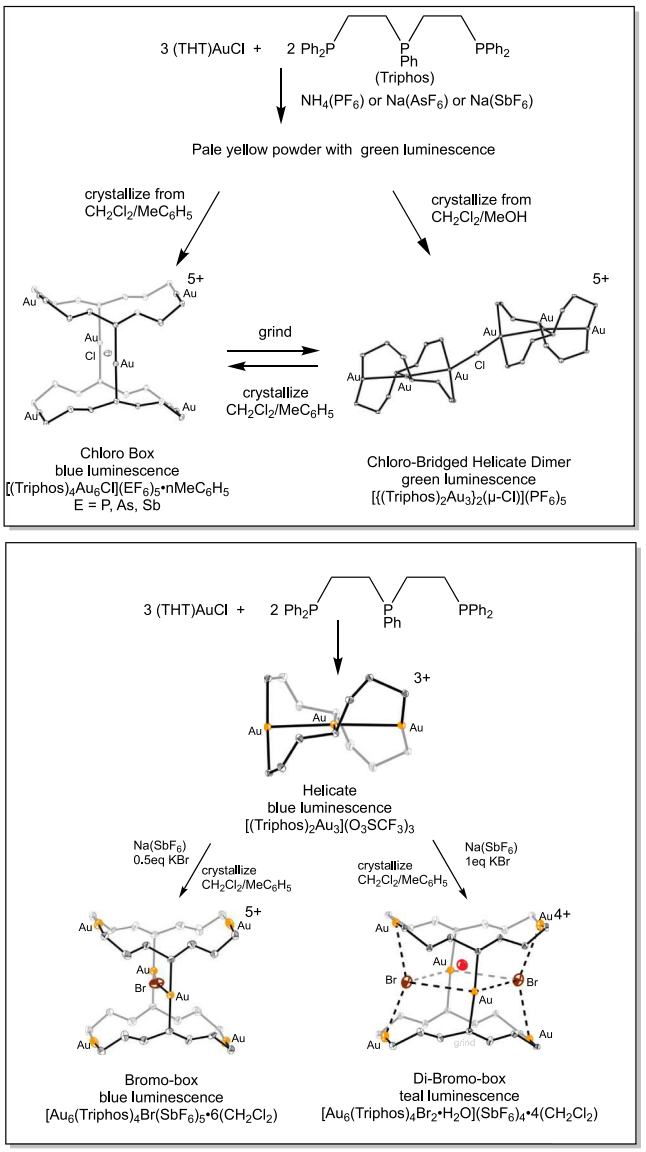

[a]Hydrogen atoms, phenyl groups, anions, and solvate molecules have been omitted for clarity.

phosphine cages to produce new luminescent compounds with metallophilic Cu/Au interactions.

A few other luminescent complexes that involve gold−copper interactions have been prepared.[27−43] For example, López-de-Luzuriaga and co-workers have constructed compounds with gold−copper interactions through the combination of the anion $[Au(C_6X_5)_2]^-$ (X = F or Cl) with cationic copper(I) complexes.[31−36] Catalano and co-workers have constructed a number of bridging ligands that bind a gold(I) ion through phosphine or carbene donors and have pyridyl groups that can coordinate one or two copper(I) ions.[37−42] In these complexes, the distance between the copper and gold centers can be manipulated by changing the number and kinds of additional ligands that bind to the copper(I) ions. Unbridged complexes in which two cyclic, trinuclear molecules are linked together through the formation of Au(I)−Cu(I) bonds have been prepared by Omary and co-workers.[43]

RESULTS AND DISCUSSION

Preparation and Structure of $[Au_6(Triphos)_4(CuBr_2)](OTf)_5\cdot(CH_2Cl_2)_3\cdot(CH_3OH)_3\cdot(H_2O)_4$ (1) and $[Au_6(Triphos)_4(CuCl_2)](PF_6)_5\cdot(CH_2Cl_2)_4$ (2). The preparative work is summarized in Scheme 2. A sample of colorless

Scheme 2. Formation of Copper and Gold Box Pentacations[a]

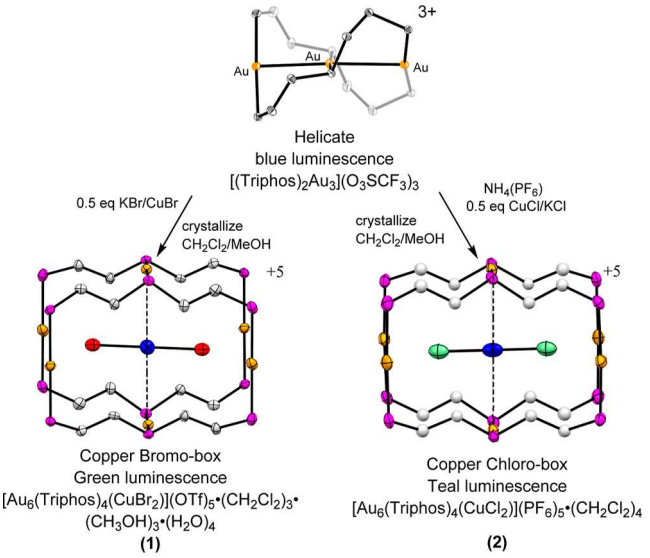

[a]Hydrogen atoms, phenyl groups, anions, and solvate molecules have been omitted for clarity. Color scheme: Au, orange; Cu, blue; Br, red; Cl, green; C, gray or white; P, pink.

$[Au_6(Triphos)_4(CuBr_2)](OTf)_5\cdot(CH_2Cl_2)_3(CH_3OH)_3\cdot(H_2O)_4$ (1) was obtained by adding a solution of $K(CuBr_2)$ in methanol to a dichloromethane solution of the helicate $[Au_3(Triphos)_2](OTf)_3$ in a process similar to that used for the preparation of the bromo-box and di-bromo-box as shown in the lower part of Scheme 1. The colorless product displayed green luminescence under UV irradiation. Crystallization was achieved by the diffusion of diethyl ether into a methanol/dichloromethane solution of the product. Colorless crystals of $[Au_6(Triphos)_4(CuCl_2)](PF_6)_5\cdot(CH_2Cl_2)_4$ (2) were obtained by a self-assembly process that involved mixing a solution of Triphos in dichloromethane with a solution of CuCl in acetonitrile, followed by the addition of a dichloromethane solution of Au(tht)Cl (tht = tetrahydrothiophene) and finally addition of solid $(NH_4)(PF_6)$. After stirring and evaporation of the solvent, the product was extracted with dichloromethane and recrystallized by slow layer diffusion of ether into the dichloromethane solution. Under UV light, these crystals had a teal luminescence. Crystals of $[Au_6(Triphos)_4(CuBr_2)](OTf)_5\cdot(CH_2Cl_2)_3(CH_3OH)_3\cdot(H_2O)_4$ (1) and of $[Au_6(Triphos)_4(CuCl_2)](PF_6)_5\cdot(CH_2Cl_2)_4$ (2) are quite fragile, particularly when removed from their mother liquor. Away from the mother liquor, they crack and crumble, presumably due to the loss of volatile solvate molecules. Solvate loss from crystals is a serious issue that can alter not only composition but also structure and properties.[44] The low solubility and solution instability of these crystals preclude characterization by liquid-phase techniques such as NMR spectroscopy.

Crystals of $[Au_6(Triphos)_4(CuBr_2)](OTf)_5\cdot(CH_2Cl_2)_3\cdot(CH_3OH)_3\cdot(H_2O)_4$ (1) contain two independent cations in the asymmetric unit. Figure 1 shows drawings of these two

https://doi.org/10.1021/acs.inorgchem.2c04067
Inorg. Chem. 2023, 62, 4467−4475

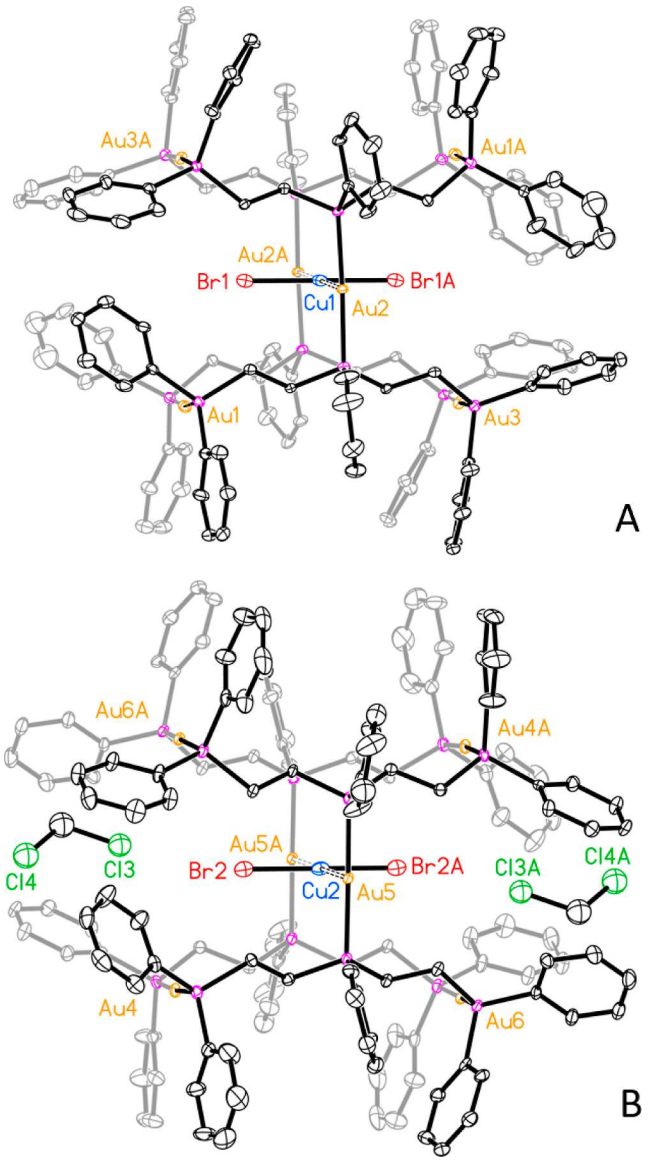

Figure 1. Structures of the two different cations, A and B, $[Au_6(Triphos)_4\ (CuBr_2)]^{5+}$ in $[Au_6(Triphos)_4(CuBr_2)](OTf)_5\cdot(CH_2Cl_2)_3\cdot(CH_3OH)_3\cdot(H_2O)_4$ (**1**) drawn with thermal contours at the 50% probability level. For cation B, containing Cu2, two molecules of dichloromethane reside within the box, while there are no dichloromethane molecules inside cation A that contains Cu1. For clarity, hydrogen atoms, the anions, and the other dichloromethane molecule and the methanol molecules have been omitted.

cations, which will be known as cation A or B. Some interatomic distances in these cations are compiled in Table 1. Each cation is centrosymmetric, with the copper ion residing on a crystallographic center of symmetry. The overall shape of the box is similar to those of the chloro and bromo boxes shown in Scheme 1. The six gold ions are widely dispersed, indicating that there are no aurophilic contacts in the box. The Au−P distances in the two cations fall in a narrow range, 2.294(2) to 2.309(2) Å. The Cu−Br distances [2.2353(10) and 2.2320(11) Å] in the two cations are similar and typical for other examples of this ion. The average Cu−Br distance in the 56 examples of the $[CuBr_2]^-$ ion deposited in the CCDC is 2.230[6] Å.[45] In contrast, the Au−Cu distances in the two cations differ: that distance is 3.2172(4) Å in cation A and 3.0738(4) Å in cation B. In cation B, there are two molecules of dichloromethane that reside within the box, while no solvate molecules are found within the confines of cation A.

Since it is unusual for two instances of the same molecule in the same crystal structure to have distances that differ by >0.1 Å, we decided to investigate the energetics of these species using DFT. Single-point calculations on the bare pentacations fixed to their crystallographic geometries revealed a rather large energetic difference of 58.06 kJ/mol, the structure with the *long* Au−Cu, cation A, distance being more stable. This energy difference between cation A and cation B geometries is too large to be accounted for by normal packing forces, so we looked beyond the molecule for a possible explanation. Analysis of the crystal structure revealed triflate counterions positioned nearby the facial Au atoms. The distance between the nearest triflate O atom and the facial Au atom is 2.966(12) Å for cation A and 3.7905(4) Å for cation B. Figure 2 shows the location of one of the triflate ions near Au2 in cation A. By including the two triflate anions located adjacent to these facial Au atoms in the calculations, the energetic difference dropped to 4.42 kJ/mol, with cation A still being more stable. From these calculations, we propose that the difference in the Au−Cu lengths between cations A and B arises from a weak interaction between the Au center and the triflate anion. In cation A, this Au−triflate interaction stabilizes the box at the cost of the Au−Cu interaction (as seen by the bond elongation). Whereas in cation B, the Au−triflate interaction is almost non-existent due to physical separation, resulting in a less stable box that favors a stronger and shorter Au−Cu interaction.

The structure of the sole cation in the colorless crystals of $[Au_6(Triphos)_4(CuCl_2)](PF_6)_5\cdot(CH_2Cl_2)_4$ (**2**) is shown in Figure 3. Again, the cation is centrosymmetric, with Cu1

Table 1. Selected Bond Distances (Å) and Angles (°) for the Box Cations $[Au_6(Triphos)_4(CuX_2)]^{5+}$

compound	$[Au_6(Triphos)_4(CuBr_2)]^{5+}$ cation A in (**1**)	$[Au_6(Triphos)_4(CuBr_2)]^{5+}$ cation B in (**1**)	$[Au_6(Triphos)_4(CuCl_2)]^{5+}$ in (**2**)
Au2−Cu1	3.2172(4)	3.0738(4)	3.1646(10)
Cu1−X	2.2353(10)	2.2320(11)	2.104(4)
Au1−P1	2.298(2)	2.294(2)	2.300(3)
Au1−P6	2.297(2)	2.298(2)	2.305(3)
Au2−P2	2.2992(18)	2.300(2)	2.304(2)
Au2−P5	2.3080(18)	2.301(2)	2.305(3)
Au3−P3	2.2983(19)	2.307(2)	2.301(3)
Au3−P4	2.3056(19)	2.309(2)	2.297(3)
Au2···Au2A (width)	6.434	6.147	6.329
Au1···Au3 (length)	8.230	8.438	8.357
Au1···Au3A (depth)	7.357	7.1861	7.386

https://doi.org/10.1021/acs.inorgchem.2c04067
Inorg. Chem. 2023, 62, 4467−4475

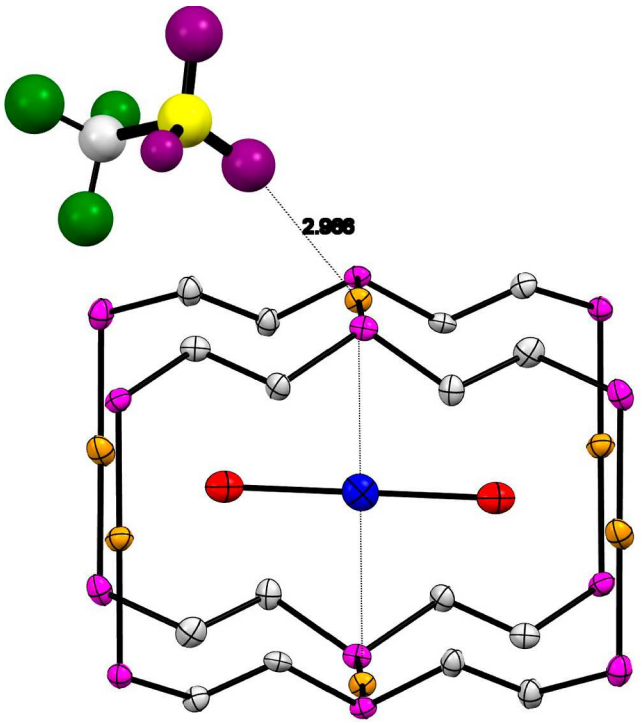

Figure 2. Positioning of a triflate ion near Au2 in cation A in $[Au_6(Triphos)_4(CuBr_2)](OTf)_5\cdot(CH_2Cl_2)_3\cdot(CH_3OH)_3\cdot(H_2O)_4$ (**1**) drawn with thermal contours at the 50% probability level. For clarity, hydrogen atoms, phenyl groups, other anions, and the dichloromethane and methanol molecules have been omitted. Color scheme: Au, orange; Cu, blue; Br, red; Cl, green; C, gray or white; P, pink; F, green; S, yellow; O, violet.

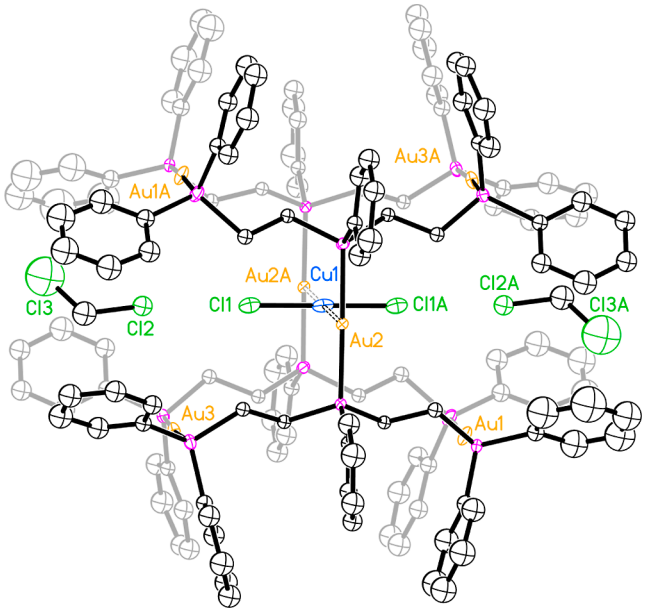

Figure 3. Structure of the cation $[Au_6(Triphos)_4(CuCl_2)]^{5+}$ in $[Au_6(Triphos)_4(CuCl_2)](PF_6)_5\cdot(CH_2Cl_2)_4$ (**2**) along with two dichloromethane solvate molecules drawn with thermal contours at the 50% probability level. For clarity, hydrogen atoms, the anions, and the other solvate molecules have been omitted.

residing on a crystallographic center of symmetry. As seen in Table 1, the general dimensions of the cation are similar to those of the analogue, $[Au_6(Triphos)_4(CuBr_2)](OTf)_5\cdot(CH_2Cl_2)_3\cdot(CH_3OH)_3\cdot(H_2O)_4$ (**1**). The Cu−Cl distance [2.104(4) Å] falls close to the average Cu−Cl distance of 2.09(3) Å in the 219 examples of the $[CuCl_2]^-$ ion deposited in the CCDC. Thus, the cage environment does not significantly alter the geometry of the $[CuCl_2]^-$ ion.

Spectroscopic Properties. The emission and excitation spectra of colorless crystals of $[Au_6(Triphos)_4(CuBr_2)](OTf)_5\cdot(CH_2Cl_2)_3\cdot(CH_3OH)_3\cdot(H_2O)_4$ (**1**) display a green luminescence [λ_{max}(emission), 527; λ_{max}(excitation), 318 nm] under irradiation with UV light, while crystals of $[Au_6(Triphos)_4(CuCl_2)](PF_6)_5\cdot(CH_2Cl_2)_4$ (**2**) produce teal emission [λ_{max}(emission), 464; λ_{max}(excitation), 353 nm] at room temperature. The emission and excitation spectra of these two solids are clearly different, as shown in Figure 4.

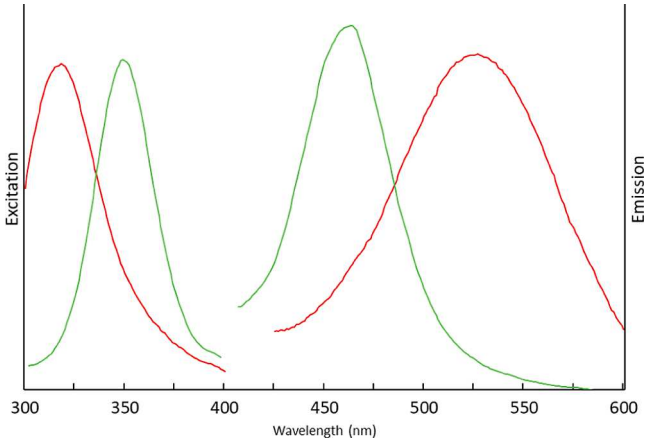

Figure 4. Emission and excitation spectra of crystals of $[Au_6(Triphos)_4(CuBr_2)]\text{-}(OTf)_5\cdot(CH_2Cl_2)_3\cdot(CH_3OH)_3\cdot(H_2O)_4$ (**1**) in red (emission obtained with excitation at 318 nm, excitation obtained for emission at 527 nm) and $[Au_6(Triphos)_4(CuCl_2)]\text{-}(PF_6)_5\cdot(CH_2Cl_2)_4$ (**2**) in green (emission obtained with excitation at 353 nm, excitation obtained for emission at 464 nm) at room temperature.

Both solids display large Stokes shifts, which are indicative of the emissions being due to phosphorescence. At room temperature, the emission lifetime is 24 μs for $[Au_6(Triphos)_4(CuBr_2)](OTf)_5\cdot(CH_2Cl_2)_3\cdot(CH_3OH)_3\cdot(H_2O)_4$ (**1**) and 26 μs for $[Au_6(Triphos)_4(CuCl_2)](PF_6)_5\cdot(CH_2Cl_2)_4$ (**2**) These lifetimes are also consistent with both emissions being due to phosphorescence. The spectra in Figure 4 were obtained with the crystals in contact with their mother liquor to ensure crystal integrity. Notice in Figures 1 and 3 that dichloromethane molecules are inside the cationic boxes and their loss through evaporation is likely to alter the properties of the cationic complexes. At room temperature, the mother liquor was not luminescent, but upon cooling, the mother liquor became luminescent. Consequently, we could not obtain low-temperature emission and excitation spectra for these two crystals.

Computational Studies of the Au−Cu Bonding. Single-point (SP) calculations were conducted to visualize the orbitals involved in d^{10}−d^{10} bonding in order to understand the nature of the Au−Cu interaction, while time-dependent density functional theory (TD-DFT) calculations were conducted to model the excitations contributing to the photoluminescence observed in the cations, $[Au^I_6(Triphos)_4(Cu^ICl_2)]^{5+}$ in (**2**) and $[Au^I_6(Triphos)_4(Cu^IBr_2)]^{5+}$ in (**1**). In both cations, the two

https://doi.org/10.1021/acs.inorgchem.2c04067
Inorg. Chem. 2023, 62, 4467−4475

Au−Cu distances are equivalent by symmetry since the copper ions reside on an inversion center and are therefore discussed in the singular.

The nature of d^{10}−d^{10} bonding: In 1978, Dedieu and Hoffman established the theoretical framework for d^{10}−d^{10} interactions.[46] Metal−metal partial bonding between closed-shell ions arises from hybridization of the filled metal−metal σ^* orbital with empty $(n + 1)$s and p orbitals on each metal center. This hybridization adds a nonbonding character to the σ^* orbital, effectively removing antibonding contributions to the total energy while preserving the bonding character of the lower-energy σ orbital. In 1990, this framework was first applied by Arkhireeva et al. to multinuclear Cu(I) complexes.[47] This bonding interaction is often accompanied by luminescence, stemming from the excitation of an electron from the filled σ^* orbital to linear combinations (with constructive overlap) of the $(n + 1)$s and p atomic orbitals.[48] The partial d^{10}−d^{10} bonding interaction is dubbed metallophilicity.[49−51]

The Au−Cu ground state d^{10}−d^{10} bonding interaction: The Au−Cu Mayer bond orders of 0.16−0.20, Table 2, indicate a small metal−metal bonding interaction between the central copper(I) ion and the facial gold(I) ion for both cations. Consistent with the small Mayer bond orders, the formal shortness ratios (FSR, defined as the interatomic metal−metal distance divided by the sum of metallic radii) of 1.20−1.28 exceed the expected value for a single covalent metal−metal bond (1.00−1.05).[52,53] A survey of the CCDC database shows a minimum Au−Cu distance of 2.56 Å[54] with a mean distance of 3.50 Å,[45] and these distances correspond to FSR values of 1.02 and 1.39, respectively. The metallophilicity was found to vary between (**1**) and (**2**), as reflected by the range of Au−Cu distances and the span of Mayer bond orders. Since the calculated bond orders of cations A and B for 1 are so similar, the orbital analysis of only one of these, cation A, was examined in closer detail. The calculated electronic structures have highest-occupied molecular orbitals (HOMOs) that are characterized by an anti-bonding interaction between the gold(I) and copper(I) ions, for both (**1**) and (**2**), as well as hybridization between the $(n + 1)$s and p orbitals, as seen in Figures 5 and 6. Table 3 displays the orbital contributions, indicating mixing of the σ^* orbital with 4s/3d character on copper and 6s/6p/5d character on gold. This hybridization demonstrates that the Au−Cu distances in the ground state support metallophilic interactions, which are further evidenced by the observed luminescence.[55−57]

Table 2. Experimental and Computational Values Relating to the Au−Cu Interactions (2) and (1)

	crystallographic bond distance (Å)	Mayer bond order	FRS
$[Au_6(Triphos)_4(CuCl_2)]^{5+}$ Au1−Cu1 in (**2**)	3.1646(10)	0.20	1.26
$[Au_6(Triphos)_4(CuBr_2)]^{5+}$ Au3−Cu1 in (**1**) cation A	3.2172(4)	0.16	1.28
$[Au_6(Triphos)_4(CuBr_2)]^{5+}$ Au5−Cu2 in (**1**) cation B	3.0278(4)	0.19	1.20

Nature of Luminescence. Analysis of the TD-DFT outputs for (**1**) and (**2**) revealed a primary excitation around 320 nm responsible for the observed UV absorption feature as has been previously seen in other Au−Cu-containing species and consistent with the excitation spectra shown in Figure 4.[29]

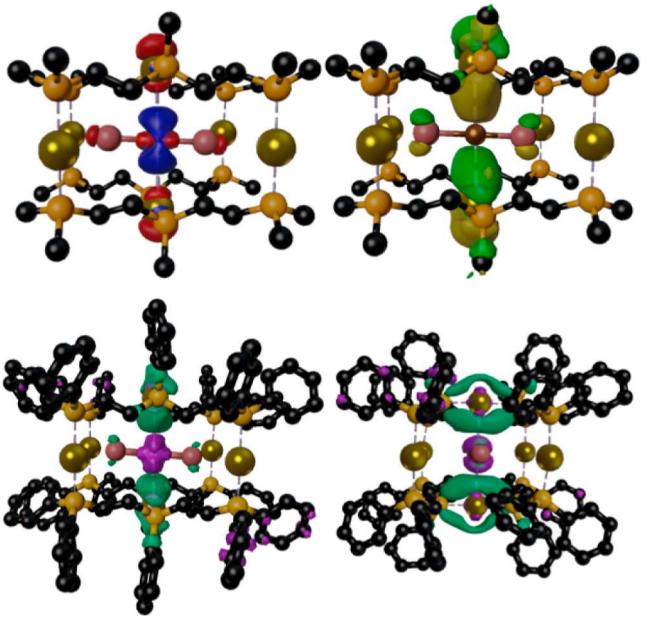

Figure 5. Top left: Filled Au−Cu σ^* orbital for $[Au_6(Triphos)_4(CuBr_2)]^{5+}$ in (**1**), which is the primary metal-based donor orbital for the observed excitation. The phenyl rings are omitted for clarity. Top right: Empty Au−Cu σ orbital, which is the primary metal-based acceptor orbital for the observed excitation. The phenyl rings are omitted for clarity. Bottom: Two views of the electron density difference map calculated for the most intense electronic excitation. Purple indicates a loss of electron density, and teal indicates a gain in electron density.

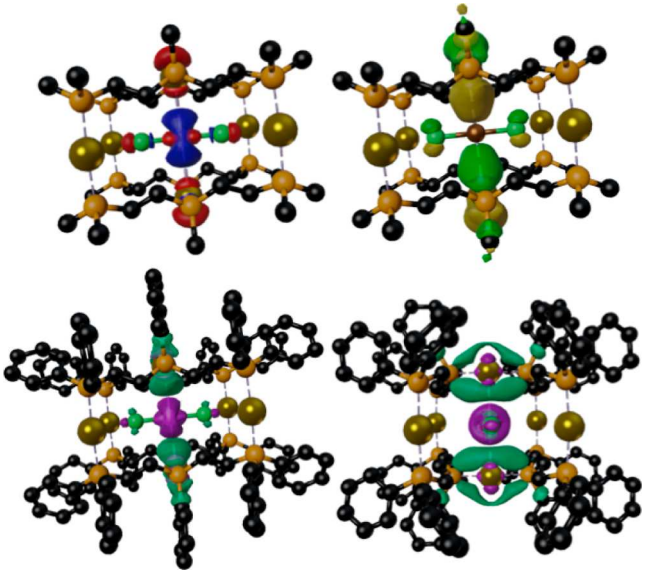

Figure 6. Top left: Filled Au−Cu σ^* orbital for $[Au_6(Triphos)_4(CuCl_2)]^{5+}$ in (**2**), which is the primary metal-based donor orbital for the observed excitation. The phenyl rings are omitted for clarity. Top right: Empty Au−Cu σ orbital, which is the primary metal-based acceptor orbital for the observed excitation. The phenyl rings are omitted for clarity. Bottom: Two views of the electron density difference map calculated for the most intense electronic excitation. Purple indicates a loss of electron density and teal indicates a gain in electron density.

For both complexes, the excitation was calculated to be a composite of multiple one-electron excitations, including

https://doi.org/10.1021/acs.inorgchem.2c04067
Inorg. Chem. 2023, 62, 4467−4475

Table 3. Percent Contributions of Atomic Orbitals to the Au−Cu Filled σ^* Donor and Empty σ Acceptor Molecular Orbitals

	atom	contributions (%)
$[Au_6(Triphos)_4(CuBr_2)]^{5+}$ σ^* donor	Cu1	3d: 54.4; 4s: 6.5
	Au2	5d: 4.8; 6s: 2; 6p: 2.8
	Au2A	5d: 4.8; 6s: 2; 6p: 2.8
$[Au_6(Triphos)_4(CuCl_2)]^{5+}$ σ^* donor	Cu1	3d: 56.4; 4s: 8.4
	Au2	5d: 5.5; 6s: 2; 6p: 3.5
	Au2A	5d: 5.5; 6s: 2; 6p: 3.5
$[Au_6(Triphos)_4(CuBr_2)]^{5+}$ σ acceptor	Cu1	4p: 11.8
	Au2	4f: 0.1; 5d: 0.3; 6p: 21.3
	Au2A	4f: 0.1; 5d: 0.3; 6p: 21.3
$[Au_6(Triphos)_4(CuCl_2)]^{5+}$ σ acceptor	Cu1	4p: 12.8
	Au2	4f: 0.2; 5d: 0.3; 6p: 22.4
	Au2A	4f: 0.2; 5d: 0.3; 6p: 22.4

ligand-to-metal and metal-to-metal charge-transfer transitions. The primary contribution to the absorption feature is a metal-to-metal (Cu-to-Au) charge transfer, as seen in Figures 5 and 6. This charge transfer originates from the filled Au−Cu weakly antibonding orbital, described above in Table 3, donating into an empty Au−Cu weakly bonding orbital, as seen in the electron difference density plots in Figures 5 and 6. Full orbital decomposition is given in Table S1. The acceptor orbital comprises a 4p orbital on the copper ion, with bonding overlap with the primarily 6p orbitals on the gold ion. This suggests that the excitation increases the strength of the Au−Cu metal−metal bonding interaction in the excited state, a hallmark of metallophilic luminescence.[37−58]

CONCLUSIONS

Two new self-assembled box-like complexes, $[Au_6(Triphos)_4(CuBr_2)](OTf)_5\cdot(CH_2Cl_2)_3\cdot(CH_3OH)_3\cdot(H_2O)_4$ (**1**) and $[Au_6(Triphos)_4(CuCl_2)](PF_6)_5\cdot(CH_2Cl_2)_4$ (**2**), have been prepared and structurally characterized. It is quite noteworthy that a single copper ion manages to become centered within the box-like cavity produced by the combination of four Triphos ligands and six gold(I) ions. This arrangement produces an unusual situation in which a CuX_2^- unit is suspended between two Au(I) centers without the intervention of bridging ligands. The Au···Cu distances in these boxes, which range from 3.0738(4) to 3.2172(4), are significantly longer than the Au···Cu distances in unbridged complexes such as $[Au(C_6F_5)_2][Cu(N{\equiv}CCH_3)_2]$ with an Au−Cu distance of 2.9335(11) Å and $[Au(C_6F_5)_2][Cu(N{\equiv}C{-}CH{=}CHPh)_2]$ with an Au−Cu distance of 2.6727(4) Å.[32] In the centrosymmetric, ligand-bridged complex, $[Au(im\text{-}(CH_2py)_2)_2(Cu(MeCN)_2)_2](PF_6)_3$, with two ligands attached to each copper(I) ion, the Au−Cu distance (4.591 Å) is too long for a metallophilic interaction, but upon exchange of the two acetonitrile ligands on each copper(I) for a single methanol molecule, the Au···Cu distance shrinks to 2.7915(7) Å, which is shorter than found in the box complexes reported here.[37] Perhaps the most relevant comparison involves the columnar structure formed by self-association of the cyclic molecule, $Au_2(\mu\text{-}C^2,N^3\text{-}BzIm)_2Cu(\mu\text{-}3,5\text{-}(CF_3)_2Pz)$.[43] In this case, the cyclic molecules associate through the formation of Au···Cu···Au chains with an Au···Cu distance of 3.317 Å, which is longer than the corresponding distances in the copper boxes reported here.

The portions of the copper/gold box pentacations that are connected through metallophilic interactions have been thoroughly analyzed in computational studies. These studies show that the excitation involved in the luminescence of these boxes results from a charge transfer from the filled Au−Cu−Au orbital, which is weakly antibonding, to an empty Au−Cu−Au orbital that is weakly bonding. Thus, the strength of the Au−Cu−Au bonding is increased in the excited state. It is remarkable that the ions trapped within these box-like structures include simple nucleophiles like chloride and bromide ions as well as copper(I)-containing anions with an electrophilic metal that directly interacts with the two adjacent gold(I) ions.

EXPERIMENTAL SECTION

Preparation of Compounds. The gold helicate $[Au_3(Triphos)_2](F_3CSO_3)_3$[26] and (tht)AuCl[59] were synthesized as previously reported. Bis(2-diphenylphosphinoethyl)phenylphosphine (Triphos), methanol, toluene, and dichloromethane were purchased from Sigma-Aldrich Co. LLC. Chloroauric acid and thallium triflate were purchased from Strem Chemicals, Inc. Thallium salts are toxic and should be handled carefully. Ammonium hexafluorophosphate was purchased from Alfa Aeser, Inc. Potassium bromide was purchased from Mallinckrodt, Inc. Solids were used as received. Solvents were used as received, and all reactions were conducted on the bench top open to the atmosphere.

Synthesis of $[Au_6(Triphos)_4(CuBr_2)](OTf)_5\cdot(CH_2Cl_2)_3\cdot(CH_3OH)_3\cdot(H_2O)_4$ (1). Copper(I) bromide (8.3 mg, 0.058 mmol) and potassium bromide (6.9 mg, 0.058 mmol) were dissolved in 8 mL of methanol and 2 mL of dichloromethane under agitation, then sonicated, resulting in a blue-green solution with some very minor blue solid particulates. $[Au_3(Triphos)_2](OTf)_3$ (243 mg, 0.115 mmol) was dissolved in 4 mL of dichloromethane and added to the stirring methanolic CuBr/KBr solution. Upon addition of the $[Au_3(Triphos)_2](OTf)_3$, the solution briefly turned brown, then returned to the previously reported light blue-green color. A drop of this solution was placed on a watch glass, and the resultant yellow residue luminesced a vibrant yellow-green. The solution was then allowed to dry. The dried vial contained a predominantly yellow residue with a small amount of blue-green solid on the bottom. The residue was re-dissolved in 2 mL methanol and 5 mL dichloromethane and recrystallized by diffusion of diethyl ether. This procedure produced single-crystal X-ray diffraction quality colorless plates in 2 days, yield 63 mg, 23%. The water in the crystals originated from the methanol, which was not dried prior to use.

Infrared spectrum (cm^{-1}): 3055 (w), 2954 (w), 2924 (w), 1619 (w), 1586 (w), 1574 (w), 1483 (m), 1436 (s), 1406 (m), 1334 (vw), 1253 (vs), 1224 (s), 1153 (s), 1102 (s), 1071 (w), 1028 (vs), 998 (m), 922 (vw), 842 (w), 792 (w), 740 (s), 722 (s), 692 (vs), 636 (vs), 573 (m), 515 (vs), 480 (s), 435 (m).

Synthesis of $[Au_6(Triphos)_4(CuCl_2)](PF_6)_5\cdot(CH_2Cl_2)_4$ (2). A 4.6 mg (0.046 mmol) portion of copper(I) chloride was crushed and dissolved into 4 mL acetonitrile by sonication. Separately, a 10 mL dichloromethane solution containing 97.0 mg (0.181 mmol) of Triphos was made, and another solution was made by dissolving 87.4 mg of (tht)AuCl (0.264 mmol) in 4 mL of dichloromethane. The Triphos-containing solution was added to the copper(I) chloride solution under high agitation, and then the solution of (tht)AuCl was added. The resulting mixture was transparent and displayed blue luminescence upon UV irradiation. This solution was allowed to stir for 30 min. At this point, 413 mg (2.53 mmol) of NH_4PF_6 was added. This process resulted in the formation of a faint green suspension displaying identical luminescence, which was covered and allowed to stir for 24 h. Afterward, the suspension was filtered and transferred into a round-bottom flask, then dried by rotary evaporation. Throughout the drying process, both blue and teal luminescence were observed in the flask. Once the drying process had been completed, only teal luminescence was observed. This new solid was

https://doi.org/10.1021/acs.inorgchem.2c04067
Inorg. Chem. 2023, 62, 4467−4475

washed with a small volume of dichloromethane and sonicated briefly before filtering off the insoluble excess salts. This solution was then dried again by rotary evaporation and weighed (115.7 mg, 63% yield). The product was once more dissolved into dichloromethane and recrystallized by slow diffusion of toluene to yield colorless blocks of the product.

Infrared spectrum (cm^{-1}): 3055 (w), 3015 (w), 2899 (w), 1635 (m, b), 1585 (w), 1482 (s), 1436 (vs), 1403 (s), 1336 (w), 1309 (w), 1280 (w), 1233 (w, b), 1187 (w), 1161 (w), 1120 (m), 1098 (s), 1057 (m), 971 (s), 872 (s), 846 (w), 786 (m), 736 (s), 717 (w), 687 (vs), 657 (m, b), 614 (w), 556 (w), 511 (vs), 477 (vs), 447 (vs).

Alternative Synthesis of $[Au_6(Triphos)_4(CuCl_2)](PF_6)_5 \cdot (CH_2Cl_2)_4$ (2). A 29.3 mg (0.295 mmol) portion of copper(I) chloride was dissolved in 40 mL of acetonitrile, and a solution of Triphos (217 mg, 0.406 mmol) in 40 mL of dichloromethane was added to this solution. The reaction proceeded for 2 h and was followed by the addition of the solution of [Au(tht)Cl] (94.9 mg, 0.295 mmol) in 40 mL of dichloromethane. The reaction mixture was stirred for 1 h, followed by the addition of an excess amount of ammonium hexafluorophosphate (643 mg, 3.94 mmol) as a solid. The reaction mixture was stirred for an additional hour. After evaporation of the solvent, the product was extracted by 40 mL of dichloromethane and recrystallized by slow diffusion of a layer of ether into the product solution in dichloromethane. The product was obtained as colorless blocks the same as produced in the first synthesis, having the same emission and excitation spectra. Yield: 69.3% (142.9 mg).

X-ray Crystallography and Data Collection. Crystals were coated with a hydrocarbon oil after being transferred with a covering of mother liquor to a microscope slide. A colorless plate of $[Au_6(Triphos)_4(CuBr_2)](OTf)_5 \cdot (CH_2Cl_2)_3 \cdot (CH_3OH)_3 \cdot (H_2O)_4$ (**1**) was mounted in the 100 K nitrogen cold stream produced by an Oxford Cryostream low temperature apparatus on the goniometer head of a Bruker D8 Venture Kappa DUO diffractometer equipped with a Bruker Photon 100 CMOS detector and a MoKα microsource. A colorless block of $[Au_6(Triphos)_4(CuCl_2)](PF_6)_5 \cdot (CH_2Cl_2)_4$ (**2**) was mounted in the 90 K nitrogen cold stream provided by a Cryo Industries low-temperature apparatus on the goniometer head of a Bruker APEX II sealed-tube diffractometer and CCD detector with the use of MoKα (λ = 0.71073 Å) radiation. A multi-scan absorption correction was applied with the program SADABS.[60] The structures were solved by a dual space method (SHELXT)[61] and refined by full-matrix least-squares on F^2 (SHELXL-2017).[62] CCDC 2068539−2068540 contain the supplementary crystallographic data for this paper.

Physical Measurements. IR spectra were recorded on a Bruker Alpha FT-IR spectrometer using attenuated total reflectance (ATR). Fluorescence excitation and emission spectra were recorded on a PerkinElmer LS50B luminescence spectrophotometer.

Computational Methods. Density-functional theory (DFT) calculations were carried out using ORCA version 4.0.0.2.[63] The crystallographic coordinates were used without further optimization. For single-point calculations, the BP86[64] exchange−correlation functional and the resolution of identity (RI)[65] approximation were used. The segmented all-electron relativistically contracted (SARC) basis set, SARC-DKH-TZVPP,[66−68] was used for the Au atoms. The relativistically recontracted Karlsruhe basis set, DKH-def2-TZVPP,[46] was used for Cu and Br atoms, while DKH-def2-SVP[45,69] was used for all other atoms. The auxiliary coulomb basis set, SARC/J,[44] was used for all atoms. Dispersion corrections to the calculations were accounted for with the atom pairwise dispersion correction employing the Becke−Johnson damping scheme (D3BJ).[70,71] All self-consistent field calculations used Grid4 (Lebedev quadrature with 302 points) and FinalGrid5 (Lebedev quadrature with 434 points) for numerical integration. Time-dependent DFT calculations were done for 150 roots, with a Davidson expansion space of 1500, and a convergence criterion of 10^{-4} au. Visualizations of the orbitals from self-consistent field calculations were carried out with the UCSF Chimera package and Blender.[72]

■ ASSOCIATED CONTENT

Supporting Information

The Supporting Information is available free of charge at https://pubs.acs.org/doi/10.1021/acs.inorgchem.2c04067.

Details of computational studies (PDF)

Accession Codes

CCDC 2068539−2068540 contain the supplementary crystallographic data for this paper. These data can be obtained free of charge via www.ccdc.cam.ac.uk/data_request/cif, or by emailing data_request@ccdc.cam.ac.uk, or by contacting The Cambridge Crystallographic Data Centre, 12 Union Road, Cambridge CB2 1EZ, UK; fax: +44 1223 336033.

■ AUTHOR INFORMATION

Corresponding Authors

John F. Berry − *Department of Chemistry, University of Wisconsin-Madison, Madison, Wisconsin 53706, United States;* orcid.org/0000-0002-6805-0640; Email: berry@chem.wisc.edu

Alan. L. Balch − *Department of Chemistry, University of California-Davis, Davis, California 05616, United States;* orcid.org/0000-0002-8813-6281; Email: albalch@ucdavis.edu

Authors

Daniel T. Walters − *Department of Chemistry, University of California-Davis, Davis, California 05616, United States*

Michael M. Aristov − *Department of Chemistry, University of Wisconsin-Madison, Madison, Wisconsin 53706, United States;* orcid.org/0000-0003-1161-5126

Reza Babadi Aghakhanpour − *Department of Chemistry, University of California-Davis, Davis, California 05616, United States;* orcid.org/0000-0002-8300-6322

Daniel J. SantaLucia − *Department of Chemistry, University of Wisconsin-Madison, Madison, Wisconsin 53706, United States;* Present Address: Max-Planck-Institut für Kohlenforschung, Kaiser-Wilhelm-Platz 1, D-45470, Mülheim an der Ruhr, Germany; orcid.org/0000-0002-4201-6612

Sarah Costa − *Department of Chemistry, University of California-Davis, Davis, California 05616, United States*

Marilyn. M. Olmstead − *Department of Chemistry, University of California-Davis, Davis, California 05616, United States;* orcid.org/0000-0002-6160-1622

Complete contact information is available at: https://pubs.acs.org/10.1021/acs.inorgchem.2c04067

Author Contributions

Synthetic studies and crystal growth: D.T.W., R.B.A., and S.C.; crystal data collection and analysis: D.T.W. and M.M.O.; computational studies: M.M.A., D.J.S., and J.F.B.; writing: M.M.A., J.F.B., and A.L.B.

Notes

The authors declare no competing financial interest.

■ ACKNOWLEDGMENTS

We thank the National Science Foundation (grant CHE-1807637 and grant-1953924) for partial support of this project and the Grant CHE-1531193 for the dual-source X-ray diffractometer.

REFERENCES

(1) Hong, C. M.; Bergman, R. G.; Raymond, K. N.; Toste, F. D. Self-Assembled Tetrahedral Hosts as Supramolecular Catalysts. *Acc. Chem. Res.* **2018**, *51*, 2447−2455.

(2) Ward, M. D.; Hunter, C. A.; Williams, N. H. Coordination Cages Based on Bis(pyrazolylpyridine) Ligands: Structures, Dynamic Behavior, Guest Binding, and Catalysis. *Acc. Chem. Res.* **2018**, *51*, 2073−2082.

(3) Gan, M.-M.; Liu, J.-Q.; Zhang, L.; Wang, Y.-Y.; Hahn, F. E.; Han, Y.-F. Preparation and Post-Assembly Modification of Metallosupramolecular Assemblies from Poly(N-Heterocyclic Carbene) Ligands. *Chem. Rev.* **2018**, *118*, 9587−9641.

(4) Percástegui, E. G.; Ronson, T. K. J. R.; Nitschke, J. R. Design and Applications of Water-Soluble Coordination Cages. *Chem. Rev.* **2020**, *120*, 13480−13544.

(5) Johnstone, M. D.; Schwarze, E. K.; Ahrens, J.; Schwarzer, D.; Holstein, J. J.; Dittrich, B.; Pfeffer, F. M.; Clever, G. H. Desymmetrization of an Octahedral Coordination Complex Inside a Self-Assembled Exoskeleton. *Chem.—Eur. J.* **2016**, *22*, 10791−10795.

(6) Lewis, J. E. M.; Gavey, E. L.; Cameron, S. A.; Crowley, J. D. Stimuli-responsive Pd_2L_4 metallosupramolecular cages: towards targeted cisplatin drug delivery. *Chem. Sci.* **2012**, *3*, 778−784.

(7) Echeverría, R.; López-de-Luzuriaga, J. M.; Monge, M.; Moreno, S.; Olmos, M. E.; Rodríguez-Castillo, M. Lead encapsulation by a golden clamp through multiple electrostatic, metallophilic, hydrogen bonding and weak interactions. *Chem. Commun.* **2018**, *54*, 295−298.

(8) Horiuchi, S.; Moon, S.; Ito, A.; Tessarolo, J.; Sakuda, E.; Arikawa, Y.; Clever, G. H.; Umakoshi, K. Multinuclear Ag Clusters Sandwiched by Pt Complex Units: Fluxional Behavior and Chiral-at-Cluster Photoluminescence. *Angew. Chem., Int. Ed.* **2021**, *60*, 10654−10660.

(9) Cram, D. J.; Tanner, M. E.; Thomas, R. The Taming of Cyclobutadiene. *Angew. Chem., Int. Ed. Engl.* **1991**, *30*, 1024.

(10) Mal, P.; Breiner, B.; Rissanen, K.; Nitschke, J. R. White Phosphorus Is Air-Stable within a Self-Assembled Tetrahedral Capsule. *Science* **2009**, *324*, 1697−1699.

(11) Mercado, B. Q.; Olmstead, M. M.; Beavers, C. M.; Easterling, M. L.; Stevenson, S.; Mackey, M. A.; Coumbe, C. E.; Phillips, J. D.; Phillips, J. P.; Poblet, J. M.; Balch, A. L. A seven atom cluster in a carbon cage, the crystallographically determined structure of $Sc_4(\mu_3O)_3@I_h$-C_{80}. *Chem. Commun.* **2010**, *46*, 279−281.

(12) Zhang, J. Y.; Bowles, F. L.; Bearden, D. W.; Ray, W. K.; Fuhrer, T.; Ye, Y. Q.; Dixon, C.; Harich, K.; Helm, R. F.; Olmstead, M. M.; Balch, A. L.; Dorn, H. C. A missing link in the transformation from asymmetric to symmetric metallofullerene cages implies a top-down fullerene formation mechanism. *Nat. Chem.* **2013**, *5*, 880−885.

(13) Li, X.; Roselló, Y.; Yao, Y.-R.; Zhuang, J.; Zhang, X.; Rodríguez-Fortea, A.; de Graaf, C.; Echegoyen, L.; Poblet, J. M.; Chen, N. $U_2N@I_h(7)$-C_{80}: fullerene cage encapsulating an unsymmetrical U(IV)−N−U(V) cluster. *Chem. Sci.* **2021**, *12*, 282−292.

(14) Yan, X.; Wang, H.; Hauke, C. E.; Cook, T. R.; Wang, M.; Saha, M. L.; Zhou, Z.; Zhang, M.; Li, X.; Huang, F.; Stang, P. J. A Suite of Tetraphenylethylene-Based Discrete Organoplatinum(II) Metallacycles: Controllable Structure and Stoichiometry, Aggregation-Induced Emission, and Nitroaromatics Sensing. *J. Am. Chem. Soc.* **2015**, *137*, 15276−15286.

(15) Wang, J.-S.; Wu, K.; Yin, C.; Li, K.; Huang, Y.; Ruan, J.; Feng, X.; Hu, P.; Su, C.-Y. Cage-confined photocatalysis for wide-scope unusually selective [2 + 2] cycloaddition through visible-light triplet sensitization. *Nat. Commun.* **2020**, *11*, 4675.

(16) Walters, D. T.; Aghakhanpour, R. B.; Powers, X. B.; Ghiassi, K. B.; Olmstead, M. M.; Balch, A. L. Utilization of a Nonemissive Triphosphine Ligand to Construct a Luminescent Gold(I)-Box That Undergoes Mechanochromic Collapse into a Helical Complex. *J. Am. Chem. Soc.* **2018**, *140*, 7533−7542.

(17) Walters, D. T.; Powers, X. B.; Olmstead, M. M.; Balch, A. L. The Preparation of Luminescent, Mechanochromic Molecular Containers from Non-Emissive Components: The Box Cations, $[Au_6(Triphos)_4Br]^{5+}$ and $[Au_6(Triphos)_4Br_2]^{4+}$. *Chem.—Eur. J.* **2019**, *25*, 3849−3857.

(18) Assefa, Z.; Staples, R. J.; Fackler, J. P., Jr. Bis(1,3,5-triaza-7-phosphaadamantane-P)gold(I) Chloride. *Acta Crystallogr., Sect. C: Cryst. Struct. Commun.* **1996**, *52*, 305−307.

(19) Sinha, P.; Wilson, A. K.; Omary, M. A. Beyond a T-Shape. *J. Am. Chem. Soc.* **2005**, *127*, 12488−12489.

(20) Barakat, K. A.; Cundari, T. R.; Omary, M. A. Jahn−Teller Distortion in the Phosphorescent Excited State of Three-Coordinate Au(I) Phosphine Complexes. *J. Am. Chem. Soc.* **2003**, *125*, 14228−14229.

(21) Balch, A. L. Dynamic Crystals: Visually Detected Mechanochemical Changes in the Luminescence of Gold and Other Transition-Metal Complexes. *Angew. Chem., Int. Ed.* **2009**, *48*, 2641−2644.

(22) Sagara, Y.; Yamane, S.; Mitani, M.; Weder, C.; Kato, T. Mechanoresponsive Luminescent Molecular Assemblies: An Emerging Class of Materials. *Adv. Mater.* **2016**, *28*, 1073−1095.

(23) Seki, T.; Ito, H. Molecular-Level Understanding of Structural Changes of Organic Crystals Induced by Macroscopic Mechanical Stimulation. *Chem.—Eur. J.* **2016**, *22*, 4322−4329.

(24) Xue, P.; Ding, J.; Wang, P.; Lu, R. Recent progress in the mechanochromism of phosphorescent organic molecules and metal complexes. *J. Mater. Chem. C* **2016**, *4*, 6688−6706.

(25) Ariga, K.; Mori, T.; Hill, J. P. Mechanical Control of Nanomaterials and Nanosystems. *Adv. Mater.* **2012**, *24*, 158−176.

(26) Schuh, W.; Kopacka, H.; Wurst, K.; Peringer, P. Observation of a P/M interconversion of a gold−phosphine helicate via ^{31}P NMR. *Chem. Commun.* **2001**, 2186−2187.

(27) Hobbollahi, E.; List, M.; Hupp, B.; Mohr, F.; Berger, R. J. F.; Steffen, A.; Monkowius, U. Highly efficient cold-white light emission in a $[Au_2CuCl_2(P\cap N)_2]PF_6$-type salt. *Dalton Trans.* **2017**, *46*, 3438−3442.

(28) Kobayashi, R.; Yumura, T.; Imoto, H.; Naka, K. Homo- and hetero-metallophilicity-driven synthesis of highly emissive and stimuli-responsive Au(I)-Cu(I) double salts. *Chem. Commun.* **2021**, *57*, 5382−5385.

(29) Crespo, O.; Gimeno, M. C.; Laguna, A.; Larraz, C.; Villacampa, M. D. Highly Luminescent Gold(I)-Silver(I) and Gold(I)-Copper(I) Chalcogenide Clusters. *Chem.—Eur. J.* **2007**, *13*, 235−246.

(30) Koshevoy, I. O.; Karttunen, A. J.; Tunik, S. P.; Jänis, J.; Haukka, M.; Melnikov, A. S.; Serdobintsev, P. Yu.; Pakkanen, T. A. Reversible protonation of amine-functionalized luminescent Au-Cu clusters: characterization, photophysical and theoretical studies. *Dalton Trans.* **2010**, *39*, 2676−2683.

(31) Fernández, E. J.; Laguna, A.; López-de-Luzuriaga, J. M.; Monge, M.; Montiel, M.; Olmos, M. E. Unsupported Gold(I)−Copper(I) Interactions through η_1Au-$[Au(C_6F_5)_2]^-$ Coordination to Cu^+ Lewis Acid Sites. *Inorg. Chem.* **2005**, *44*, 1163−1165.

(32) Fernández, E. J.; Laguna, A.; López-de-Luzuriaga, J. M.; Monge, M.; Montiel, M.; Olmos, M. E.; Rodríguez-Castillo, M. Unsupported Au(I)···Cu(I) interactions: influence of nitrile ligands and aurophilicity on the structure and luminescence. *Dalton Trans.* **2009**, 7509−7518.

(33) Fernandez, E. J.; Laguna, A.; Lopez-de-Luzuriaga, J. M.; Monge, M.; Montiel, M.; Olmos, M. E.; Rodriguez-Castillo, M. Solvent Induced Luminescence in Supramolecular Heterobimetallic Gold(I)-Copper(I) Complexes with a Bidentate Nitrile Ligand. *Open J. Inorg. Chem.* **2008**, *2*, 73−79.

(34) López-de-Luzuriaga, J. M.; Monge, M.; Olmos, M. E.; Pascual, P.; Rodríguez-Castillo, M. Very Short Metallophilic Interactions Induced by Three-Center-Two-Electron Perhalophenyl Ligands in Phosphorescent Au-Cu Complexes. *Organometallics* **2012**, *31*, 3720−3729.

(35) López-de-Luzuriaga, J. M.; Monge, M.; Olmos, M. E.; Pascual, D.; Rodríguez-Castillo, M. Influence of the Electronic Characteristics of N-Donor Ligands in the Excited State of Heteronuclear Gold(I)-Copper(I) Systems. *Inorg. Chem.* **2011**, *50*, 6910−6921.

https://doi.org/10.1021/acs.inorgchem.2c04067
Inorg. Chem. 2023, 62, 4467−4475

(36) Fernández, E. J.; Laguna, A.; López-de-Luzuriaga, J. M.; Monge, M.; Montiel, M.; Olmos, M. E.; Rodríguez-Castillo, M. Photophysical and Theoretical Studies on Luminescent Tetranuclear Coinage Metal Building Blocks. *Organometallics* **2006**, *25*, 3639−3646.
(37) Strasser, C. E.; Catalano, V. J. "On−Off" Au(I)···Cu(I) Interactions in a $Au(NHC)_2$ Luminescent Vapochromic Sensor. *J. Am. Chem. Soc.* **2010**, *132*, 10009−10011.
(38) Catalano, V. J.; Moore, A. L.; Shearer, J.; Kim, J. Luminescent Copper(I) Halide Butterfly Dimers Coordinated to $[Au(CH_3imCH_2py)_2]BF_4$ and $[Au(CH_3imCH_2quin)_2]BF_4$. *Inorg. Chem.* **2009**, *48*, 11362−11375.
(39) Strasser, C. E.; Catalano, V. J. Luminescent Copper(I) Halide Adducts of $[Au(im(CH_2py)_2)_2]PF_6$ Exhibiting Short Au(I)···Cu(I) Separations and Unusual Semibridging NHC Ligands. *Inorg. Chem.* **2011**, *50*, 11228−11234.
(40) Chen, K.; Nenzel, M. M.; Brown, T. M.; Catalano, V. J. Luminescent Mechanochromism in a Gold(I)-Copper(I) N-Heterocyclic Carbene Complex. *Inorg. Chem.* **2015**, *54*, 6900−6909.
(41) Chen, K.; Catalano, V. J. Luminescent Thermochromism in a Gold(I)-Copper(I) Phosphine-Pyridine Complex. *Eur. J. Inorg. Chem.* **2015**, 5254−5261.
(42) Nenzel, M. M.; Chen, K.; Catalano, V. J. Structural motifs of Au(I)-Cu(I) N-heterocyclic carbene halide complexes. *J. Coord. Chem.* **2016**, *69*, 160−167.
(43) Galassi, R.; Ghimire, M. M.; Otten, B. M.; Ricci, S.; McDougald, R. N., Jr.; Alhmoud, R. M.; Ivy, D.; Rawashdeh, J. F.; Nesterov, A.-M. M.; Reinheimer, V. N.; Daniels, E. W.; Burini, L. M.; Omary, A.; Omary, M. A. Cupriphication of gold to sensitize d^{10}-d^{10} metal-metal bonds and near-unity phosphorescence quantum yields. *Proc. Natl. Acad. Sci. U.S.A.* **2017**, *114*, E5042−E5051.
(44) Luong, L. M. C.; Lowe, C. D.; Adams, A. V.; Moshayedi, V.; Olmstead, M. M.; Balch, A. L. Seeing luminescence appear as crystals crumble. Isolation and subsequent self-association of individual $[(C_6H_{11}NC)_2Au]^+$ ions in crystals. *Chem. Sci.* **2020**, *11*, 11705−11713.
(45) Groom, C. R.; Bruno, I. J.; Lightfoot, M. P.; Ward, S. C. The Cambridge Structural Database. *Acta Crystallogr., Sect. B: Struct. Sci.* **2016**, *72*, 171−179.
(46) Dedieu, A.; Hoffmann, R. Platinum(0)-platinum(0) dimers. Bonding relationships in a d^{10}-d^{10} system. *J. Am. Chem. Soc.* **1978**, *100*, 2074−2079.
(47) Arkhireeva, T. M.; Bulychev, B. M.; Sizov, A. I.; Sokolova, T. A.; Belsky, V. K.; Soloveichik, G. L. Copper(I) complexes with metal-metal (d^{10}-d^{10}) bond. Crystal and molecular structures of adducts of tantalocene trihydride with copper(I) iodide of composition: $(\eta_5\text{-}C_5H_5)_2TaH[(\mu_2\text{-}H)Cu(\mu_2\text{-}I)_2Cu(\mu_2\text{-}H)]_2HTa(\eta_5\text{-}C_5H_5)_2$, $(\eta_5\text{-}C_5H_4But)_2TaH(\mu_2\text{-}H)_2Cu(\mu_2\text{-}I)_2Cu(\mu_2\text{-}H)_2HTa(\eta_5\text{-}C_5H_4But)_2\cdot CH_3CN$ and $\{Cu(\mu_3\text{-}I)\cdot P[N(CH_3)_2]_3\}_4$. *Inorg. Chim. Acta* **1990**, *169*, 109−118.
(48) Romanova, J.; Ranga Prabhath, M. R.; Jarowski, P. D. Relationship between Metallophilic Interactions and Luminescent Properties in Pt(II) Complexes: TD-DFT Guide for the Molecular Design of Light-Responsive Materials. *J. Phys. Chem. C* **2016**, *120*, 2002−2012.
(49) Sculfort, S.; Braunstein, P. Intramolecular d^{10}-d^{10} interactions in heterometallic clusters of the transition metals. *Chem. Soc. Rev.* **2011**, *40*, 2741−2760.
(50) Mirzadeh, N.; Privér, S. H.; Blake, A. J.; Schmidbaur, H.; Bhargava, S. K. Innovative Molecular Design Strategies in Materials Science Following the Aurophilicity Concept. *Chem. Rev.* **2020**, *120*, 7551−7591.
(51) Muñiz, J.; Wang, C.; Pyykkö, P. Aurophilicity: The Effect of the Neutral Ligand L on $[\{ClAuL\}_2]$ Systems. *Chem.—Eur. J.* **2011**, *17*, 368−377.
(52) *Multiple Bonds between Metal Atoms*, 3rd ed.; Cotton, F. A., Murillo, C. A., Walton, R. A., Eds.; Springer-Verlag: New York, 2005.
(53) Chipman, J. A.; Berry, J. F. Paramagnetic Metal-Metal Bonded Heterometallic Complexes. *Chem. Rev.* **2020**, *120*, 2409−2447.
(54) Albano, V. G.; Castellari, C.; Femoni, C.; Iapalucci, M. C.; Longoni, G.; Monari, M.; Zacchini, S. Synthesis, Chemical Characterization, and Molecular Structure of $Au_8\{Fe(CO)_4\}_4(dppe)_2$ and $Au_6Cu_2\{Fe(CO)_4\}_4(dppe)_2$. *J. Cluster Sci.* **2001**, *12*, 75−87.
(55) Ai, P.; Mauro, M.; Gourlaouen, C.; Carrara, S.; De Cola, L.; Tobon, Y.; Giovanella, U.; Botta, C.; Danopoulos, A. A.; Braunstein, P. Bonding, Luminescence, Metallophilicity in Linear Au_3 and Au_2Ag Chains Stabilized by Rigid Diphosphanyl NHC Ligands. *Inorg. Chem.* **2016**, *55*, 8527−8542.
(56) Romanova, J.; Ranga Prabhath, M. R.; Jarowski, P. D. Relationship between Metallophilic Interactions and Luminescent Properties in Pt(II) Complexes: TD-DFT Guide for the Molecular Design of Light-Responsive Materials. *J. Phys. Chem. C* **2016**, *120*, 2002−2012.
(57) King, C.; Wang, J. C.; Khan, M. N. I.; Fackler, J. P., Jr. Luminescence and metal-metal interactions in binuclear gold(I) compounds. *Inorg. Chem.* **1989**, *28*, 2145−2149.
(58) Caspar, J. V. Long-lived reactive excited states of zero-valent phosphine, phosphite, and arsine complexes of nickel, palladium and platinum. *J. Am. Chem. Soc.* **1985**, *107*, 6718−6719.
(59) Uson, R.; Laguna, A.; Laguna, M.; Briggs, D. A.; Murray, H. H.; Fackler, J. P., Jr. (Tetrahydrothiophene)gold(I) or gold(III) complexes. *Inorg. Synth.* **1989**, *26*, 85−91.
(60) Krause, L.; Herbst-Irmer, R.; Sheldrick, G. M.; Stalke, D. Comparison of silver and molybdenum microfocus X-ray sources for single-crystal structure determination. *J. Appl. Crystallogr.* **2015**, *48*, 3−10.
(61) Sheldrick, G. M. SHELXT- Integrated space-group and crystal-structure determination. *Acta Crystallogr., Sect. A: Found. Adv.* **2015**, *71*, 3−8.
(62) Sheldrick, G. M. Crystal structure refinement withSHELXL. *Acta Crystallogr., Sect. C: Struct. Chem.* **2015**, *71*, 3−8.
(63) Neese, F. Software Update: The Orca Program System, Version 4.0. *Wiley Interdiscip. Rev.: Comput. Mol. Sci.* **2018**, *8*, No. e1327.
(64) Becke, A. D. Density-Functional Exchange-Energy Approximation with Correct Asymptotic Behavior. *Phys. Rev. A: At., Mol., Opt. Phys.* **1988**, *38*, 3098−3100.
(65) Whitten, J. L. Coulombic Potential Energy Integrals and Approximations. *J. Chem. Phys.* **1973**, *58*, 4496−4501.
(66) Weigend, F. Accurate Coulomb-Fitting Basis Sets for H to Rn. *Phys. Chem. Chem. Phys.* **2006**, *8*, 1057−1065.
(67) Pantazis, D. A.; Chen, X.-Y.; Landis, C. R.; Neese, F. All-Electron Scalar Relativistic Basis Sets for Third-Row Transition Metal Atoms. *J. Chem. Theory Comput.* **2008**, *4*, 908−919.
(68) Peterson, K. A.; Puzzarini, C. Systematically Convergent Basis Sets for Transition Metals. II. Pseudopotential-Based Correlation Consistent Basis Sets for the Group 11 (Cu, Ag, Au) and 12 (Zn, Cd, Hg) Elements. *Theor. Chem. Acc.* **2005**, *114*, 283−296.
(69) Weigend, F.; Ahlrichs, R. Balanced Basis Sets of Split Valence, Triple Zeta Valence and Quadruple Zeta Valence Quality for H To Rn: Design and Assessment of Accuracy. *Phys. Chem. Chem. Phys.* **2005**, *7*, 3297−3305.
(70) Grimme, S.; Antony, J.; Ehrlich, S.; Krieg, H. A Consistent and Accurate ab initio Parametrization of Density Functional Dispersion Correction (DFT-D) for the 94 Elements H-Pu. *J. Chem. Phys.* **2010**, *132*, 154104.
(71) Grimme, S.; Ehrlich, S.; Goerigk, L. Effect of the Damping Function in Dispersion Corrected Density Functional Theory. *J. Comput. Chem.* **2011**, *32*, 1456−1465.
(72) Pettersen, E. F.; Goddard, T. D.; Huang, C. C.; Couch, G. S.; Greenblatt, D. M.; Meng, E. C.; Ferrin, T. E. UCSF Chimera? A visualization system for exploratory research and analysis. *J. Comput. Chem.* **2004**, *25*, 1605−1612.

https://doi.org/10.1021/acs.inorgchem.2c04067
Inorg. Chem. 2023, 62, 4467−4475